

INTERACTING BINARY GALAXIES. VI. THE FAST ENCOUNTER OF NGC 2672 AND NGC 2673 (KARACHENTSEV 175, ARP 167)

MARC BALCELLS

Washburn Observatory, University of Wisconsin, Madison, and Space Telescope Science Institute¹

KIRK D. BORNE²

Space Telescope Science Institute

AND

JOHN G. HOESSEL²

Washburn Observatory, University of Wisconsin, Madison

Received 1988 April 20; accepted 1988 July 1

ABSTRACT

We have studied the isolated pair of interacting ellipticals NGC 2672/2673 (Arp 167; Karachentsev 175), whose line-of-sight relative velocity is $\sim 520 \text{ km s}^{-1}$. Rotation and velocity dispersion profiles have been measured along the line connecting the galaxy centers, and broad-band CCD images have been obtained in three colors. The smaller of the two galaxies (NGC 2673; K175b; E0p) has two tidal “plumes” in its light distribution, while the larger galaxy (NGC 2672; K175a; E2) is only weakly disturbed. Velocity dispersion is roughly constant with radius in NGC 2672, but appears to increase with radius in the small galaxy, indicative of strong tidal heating. Weak counter rotation (i.e., opposite the orbital motion) is seen in NGC 2672 such that $V_{\text{rot}}/\sigma = 0.16$. The secondary galaxy (NGC 2673) has a nearly flat rotation profile along the slit, with some indication of a U-shaped component, providing evidence for the action of tidal friction. Numerical simulations have been run in order to elucidate the dynamical properties of this galactic encounter. Our models require a fast hyperbolic passage with very small pericenter separation, and they require a rapidly rotating secondary galaxy in order to produce the observed plumes on K175b. One of these plumes is straight, which is qualitatively different in appearance and origin from the usual curved tidal tails seen in colliding galaxies. Our adopted solution for K175 provides a complete dynamical description of the pair, including the spatial orientation of the orbit and its dynamical mass. The derived $M/L_B (= 7M_\odot/L_\odot^B)$ for the pair does not require a significant nonluminous contribution to the system mass.

Subject headings: galaxies: individual (NGC 2672, 2673) — galaxies: interacting — galaxies: internal motions — galaxies: photometry

I. INTRODUCTION

Although galaxy collisions involve highly complex processes, a general understanding of them has emerged from numerous investigations over the past 15 years (see White 1982 for a review, and references therein). Numerical simulations have provided an opportunity to examine these extremely nonlinear processes (Miller and Smith 1980), and to study the consequences of collisions and mergers on the structure and internal dynamics of galaxies (White 1978, 1979; Villumsen 1982; Duncan, Farouki, and Shapiro 1983; Quinn and Goodman 1986). Important insights into the internal dynamical processes that occur during the interaction, inaccessible through observation of real systems alone, have been provided by the use of numerical simulations.

Tests of our understanding of collision dynamics must involve the comparison of observations of real systems to the prediction of models which incorporate the relevant physics. In this series of papers we are studying a sample of relatively isolated interacting binary elliptical galaxies. The isolation and binary nature of the systems make their history particularly

simple. Elliptical galaxies were chosen to avoid complicated gasdynamical effects, and to simplify the ambiguity in the conversion from luminosity density to mass density: their stellar populations are more homogeneous than in spirals, and they have very little dust and gas.

The structure and internal dynamics of elliptical galaxies have been the target of much attention over the past 10 years. Our investigations are relevant to that field of research. By studying galaxies modified by an interaction we are effectively carrying out a perturbation analysis that probes the equilibrium properties of these galaxies, thus providing new constraints on their structure and dynamics.

For our study, the Karachentsev (1972) catalog of isolated binary galaxies was combed for its E-E pairs. From this set, the pairs showing strong photometric distortions were selected for detailed observation. These represent strongly interacting, physically associated systems for which CCD images and long-slit digital spectra have been obtained. Such observations provide surface brightness profiles, colors, and detailed morphological information, as well as the mean line-of-sight velocity and velocity dispersion profiles.

We attempt to model the observed pairs using the multiple three-body algorithm (or MTBA, sometimes called the semi-restricted three-body method, or the restricted N -body method; see Borne 1984, 1988a; hereafter Papers I and II, respectively). MTBA is an enhancement over the traditional

¹ Operated by the Association of Universities for Research in Astronomy, Inc., for the National Aeronautics and Space Administration.

² Visiting Astronomer, Kitt Peak National Observatory, National Optical Astronomy Observatories, operated by the Association of Universities for Research in Astronomy, Inc., for the National Science Foundation.

restricted three-body algorithm where the center of each galaxy follows a Keplerian trajectory. In MTBA, each galaxy moves subject to the forces exerted by all of the individual particles in the companion, thus allowing for tidal friction to operate. The program is equipped with extensive graphics capabilities which allow one to "observe" the structure and dynamical properties of the models during the interaction and to compare them to observational data, which consist typically of rotation, dispersion, and surface brightness profiles, as well as a quantitative description of the photometric distortions. MTBA is computationally inexpensive, which easily allows for extensive explorations of the multidimensional parameter space of a galactic encounter. Simulations can be run with up to 10,000 particles. The main results of the modeling of a real system are the orbital parameters, the three-dimensional orientation of the orbit in the sky, and the dynamical mass of the system. Important constraints can usually be found also on the internal dynamics of the colliding galaxies. Previous systems studied with this method include the pairs K99 and K564 (Borne and Hoessel 1988; Borne 1988*b*; hereafter Papers III and IV, respectively) and NGC 4782/4783 (Borne, Balcells, and Hoessel 1988; hereafter Paper V).

This paper presents a study of the pair K175 (NGC 2672/2673; Arp 167; Holmberg 99). This very unequal mass system is particularly interesting because of two low surface brightness plumes seen emerging from the secondary galaxy (NGC 2673). Little is found in the literature about NGC 2673. The primary, NGC 2672, has received more attention. It was included by Burstein (1979) in his study of absorption line strengths in elliptical and S0 galaxies. He found the spectrum of NGC 2672 to be typical of elliptical galaxies, with no traces of a young stellar population. More recently, Cutri and McAlary (1985) found that near-IR colors of both NGC 2672 and NGC 2673 show no sign of an unusual stellar population ($J-K = 1.03$ and 0.89 for NGC 2672 and 2673, respectively). Both galaxies were undetected by *IRAS* at $12\ \mu\text{m}$ (Cutri and McAlary 1985). Davis and Seaquist (1983) report an upper limit of $10.8\ \text{mJy km s}^{-1}$ for the H I 21 cm line strength, while Bieging and Biermann (1977) obtained a marginal detection which allowed them to measure a velocity but not an H I mass ($M_{\text{HI}}/L_B \leq 0.021$). NGC 2672 is a weak radio source; Feretti and Giovanini (1980) report a 408 MHz flux density of $0.06\ \text{Jy}$, while Dressel and Condon (1978) did not detect the system at 2380 MHz.

Our study focuses on the dynamics of the interaction, on the process that generated the plumes on NGC 2673, and on the properties of the system that are constrained by our modeling. The velocity measurements are significant components of the analysis. In Papers II and III we emphasized that the addition of velocity measures to detailed imaging data is required in order to fully determine the dynamical state of interacting and other disturbed galaxies (see also Paper IV). The velocity data truly act to constrain the projection factors, mass estimates, and orbital configurations of the range of simulations that are found to match all available observations for a given pair of galaxies. Papers IV and V, and Borne and Richstone (1988) demonstrate this point clearly for several interacting systems. As for the uniqueness of such solutions, Paper II argues that point in great detail for generalized collisions, while an effort is made below to prove the point specifically for the pair NGC 2672/2673.

The paper starts with the observational information. In § II we describe the photometric data, the distortions in the gal-

axies, and their photometric properties. Section III is devoted to the spectroscopic observations and to the description of the velocity structure derived from these. In § IV we present our adopted physical solution for the pair, with an outline of the rationale behind our orbit search process. In § V the uncertainties in the parameters that describe our best-fit model are discussed, and § VI analyzes the physics of plume formation as applied to NGC 2673. Results are summarized in § VII.

In this paper we will refer to the two galaxies by their Karachentsev numbers: K175a = NGC 2672 is the western component or the primary; K175b = NGC 2673 is the secondary, or eastern component of the pair. Since we will focus much attention on the distortions in the secondary, we will often refer to the primary K175a as *the perturber*.

II. BROAD-BAND IMAGING

a) Observations

Observations were carried out with the RCA No. 1 CCD at the Ritchey-Chretien (R-C) focus of the KPNO 0.9 m telescope on 1983 March 10. The seeing was $\sim 2''$ and the night was photometric, as judged from visual checks and the residuals to the standard star solutions ($\approx 1\%$). We exposed frames through the *B*, *V*, and *R* filters for 900 s each. Eight stars from the Landolt (1973) catalog were observed during the night and were used as standards. We reduced the raw data in the standard way, subtracting the bias level and then flat-fielding by using exposures of a uniformly illuminated target on the inside of the dome. An additional 600 s red exposure was obtained in 1981 October on the KPNO 2.1 m telescope using the Space Telescope wide-field/planetary camera ground-based CCD imaging system.

b) Morphology

We display our 600 s red image of the pair in a gray-scale print (Fig. 1 [Pl. 17]) and in a surface brightness contour plot (Fig. 2). K175b, the smaller member of the pair, appears to the left (east) at $37''$ from the primary core. The most prominent distortions in the system are two roughly perpendicular, low surface brightness extensions or plumes emerging from the secondary core. They are not obvious in the contour map, but the gray scale picture shows that they are two separate features; they are barely visible on the Palomar Sky Survey prints. The main plume defines an arc extending to the east from the main body of the secondary. The second plume, of lower surface brightness, is straight and extends to the north. To obtain a better image of these features, free from contamination by the primary's light, we have subtracted a model of the primary galaxy from the image of the secondary. This cannot be accomplished in a completely satisfactory way because, as discussed below, the primary has noticeable distortions also. We can, however, subtract a model that best matches the primary at the surface brightness levels where most of the superposition occurs. This does leave residual primary light in some areas of the subtracted picture, as well as oversubtracted regions, but this occurs sufficiently far from the secondary that no pollution occurs. We verified that the general sky level of the CCD image is regained in the subtracted areas immediately surrounding the secondary. A contour plot of the subtracted image is shown in Figure 3. Two pieces of information can be obtained from this picture. First, we can see the exact shape of the two plumes. Second, we see that the distortions at the secondary core are much smaller than what Figure 2 would lead us to

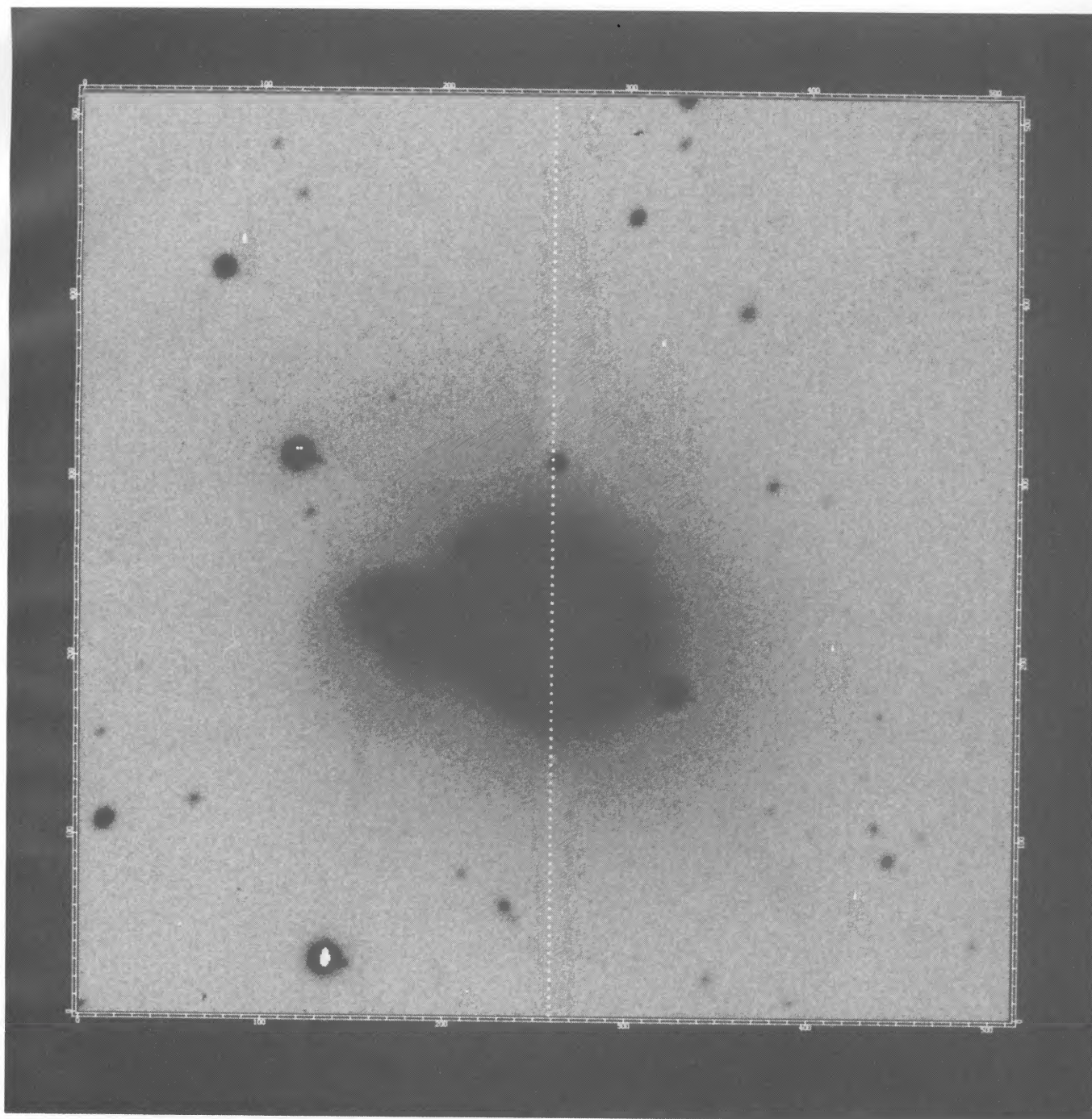


FIG. 1.—10 minute red CCD image of the K175 pair taken at the KPNO 2.1 m telescope. North is down, east is to the left (reverse from the sky). The scale of this 512×512 frame is $0''.49$ per pixel.

BALCELLS, BORNE, AND HOESSEL (see 336, 656)

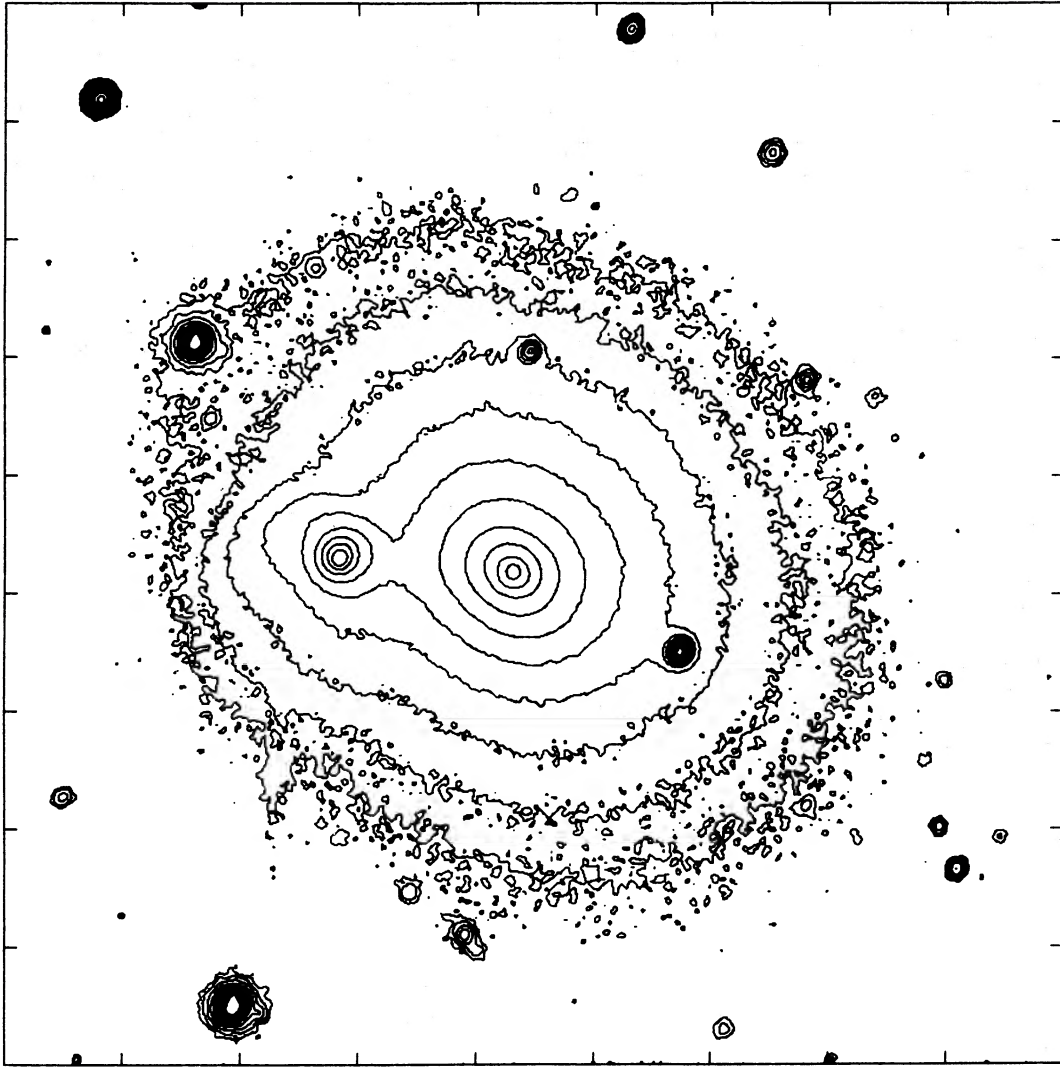


FIG. 2.—Surface brightness contours for K175. The scale is $0''.49$ per pixel, where tick marks on the boundary occur every 50 pixels. Contour intervals are drawn at $0.5R$ mag arcsec $^{-2}$ intervals. North is down, east is to the left (reverse from the sky).

believe. Once the light from the primary has been subtracted, the resulting secondary core isophotes are almost completely concentric. The small remaining core asymmetry is probably real, since the distortion is not toward the primary but in a direction roughly perpendicular to that, toward the north.

Distortions in the primary galaxy, K175a, are much smaller. It is classified as an E2 in the *Second Reference Catalogue of Bright Galaxies* (de Vaucouleurs, de Vaucouleurs, and Corwin 1976; hereafter RC2), and a deep picture (Fig. 1) first gives the impression that it is essentially an unperturbed elliptical with an inbedded or superposed companion. A detailed look at the contour plot (Fig. 2) reveals that most of the isophotes are distended toward the southeast. In the inner parts the isophotes also show noticeable deviations from ellipses. We believe that these distortions are not due to light contamination from the secondary but to the dynamic response of the stars in the primary to the passage of the secondary. Note that the appearance of the contours in Figure 2 suggests that the secondary light remains confined to a small well-defined region.

c) Surface Photometry

Given the strong superposition of the two galaxies, obtaining magnitudes for each component separately is difficult. As a tentative approach we fit seeing-convolved de Vaucouleurs profiles to the uncontaminated sectors of each galaxy. This is reasonable for the primary galaxy which has only minor distortions; we obtained an excellent fit over a range of 7 mag in surface brightness, down to $25V$ mag arcsec $^{-2}$ or 4% of the sky (Fig. 4). This was not expected since the primary isophotes show some distortion at all surface brightness levels. The mean effective radius is $30''.7$ or 9.13 kpc for $H_0 = 60$ km s $^{-1}$ Mpc $^{-1}$. The asymptotic magnitude ($V = 11.54$) agrees well with the values given in the RC2 catalog (Table 1).

For the secondary, a seeing-convolved $r^{1/4}$ fit to the inner $7''$ (down to 21.2 mag arcsec $^{-2}$) gave an asymptotic V magnitude of 13.94, corresponding to a luminosity ratio of 1:9 for the K175 pair. Beyond $7''$, contamination by the primary light and tidal distortion make the fit meaningless. The profile and the fit are shown in Figure 4. A check on the integrated V magnitude was obtained by adding all the secondary light in the primary-

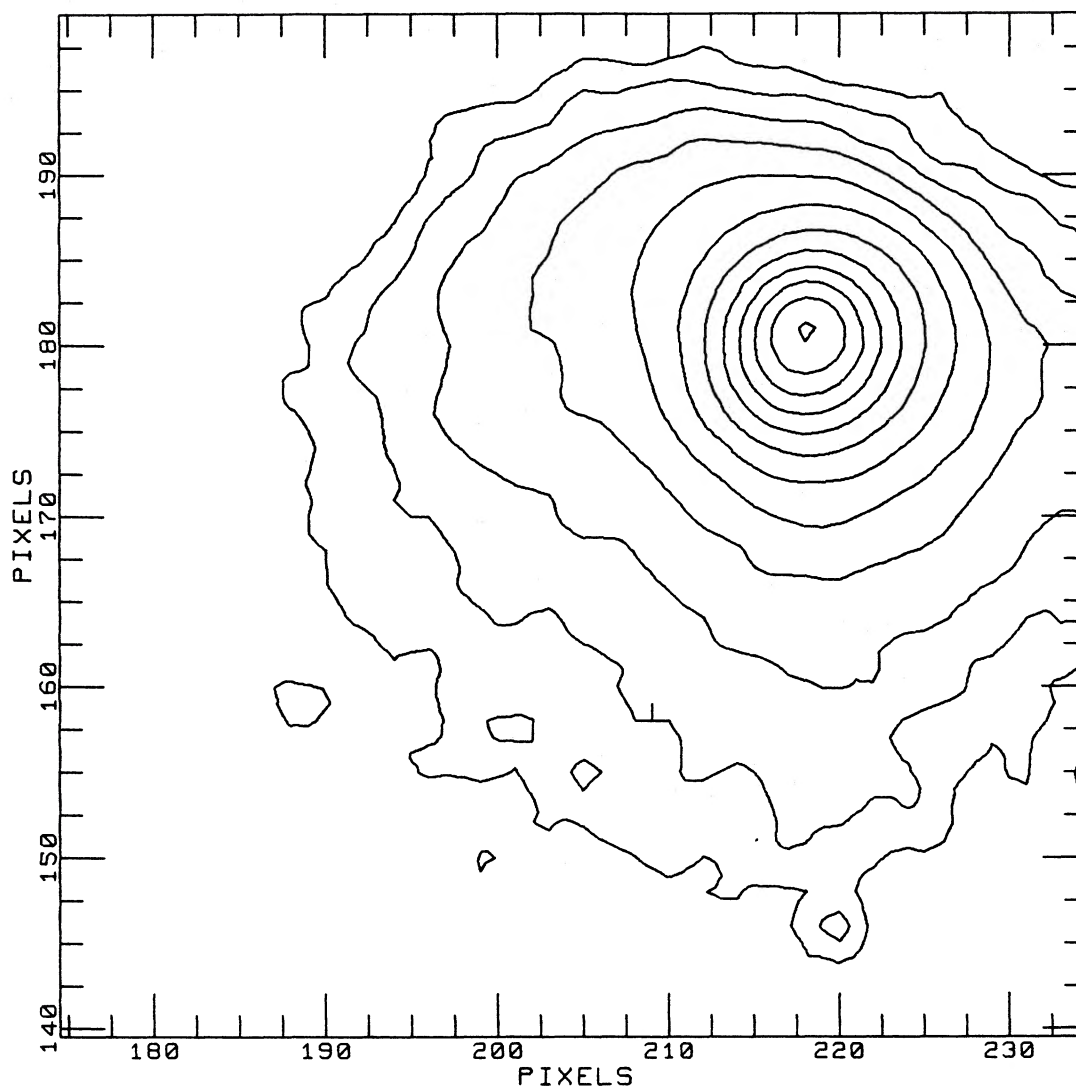


FIG. 3.—Surface brightness contours from the primary-subtracted image of the secondary. Same orientation as Figs. 1 and 2. The scale is $0''.49$ per pixel, where pixels are labeled on the axes. Contours are drawn at $0.5R$ mag arcsec $^{-2}$ intervals.

subtracted picture shown in Figure 3. The result agrees perfectly with that from the fit to the surface brightness profile.

The distance to K175, derived from the spectroscopic observations explained in the next section, is 61.3 Mpc. Absolute V magnitudes then are -22.40 and -20.00 for K175a and K175b, respectively. This places K175b in the domain of the small, rapidly rotating ellipticals (Davies *et al.* 1983). Later in the paper it will be argued that, in spite of showing no signs of rotation along the slit in our observations, the outcome of the

binary collision provides evidence that K175b is indeed a rapidly rotating elliptical.

$B-V$ colors were obtained for the two components and are listed in Table 1. They are normal for elliptical galaxies, and they agree closely with the values listed in RC2. There is no indication of a color gradient in either galaxy.

III. SPECTROSCOPIC OBSERVATIONS

Long-slit digital spectra were obtained for K175 in 1981 February using the high-gain video spectrometer (HGVS) on the KPNO 4 m telescope. The instrument and data reduction procedure were described by Kormendy and Illingworth (1982). Our analysis here follows that described in Paper III. Briefly, the SIT Vidicon detector is read out in a 128×512 pixel configuration, with the long dimension parallel to the dispersion. The slit was placed along the line connecting the centers of the two galaxies. Six 25 minute exposures were obtained, bracketed, and separated by exposures of a He-Ne-Ar comparison lamp. Each spectral frame was debiased, dark-subtracted, "flattened," distortion-corrected, wavelength-calibrated, and then sky-subtracted before all six frames were

TABLE 1
MAGNITUDES AND COLOURS

SOURCE	NGC 2672		NGC 2673	
	V	$B-V$	V	$B-V$
This work ^a	11.54 ± 0.01	1.00	13.9 ± 0.01	1.00
RC2	11.62 ± 0.13	0.98 ± 0.03	12.91 ± 0.13	0.99 ± 0.05
RSA	11.61

^a Asymptotic magnitudes from the $r^{1/4}$ fits discussed in the text.

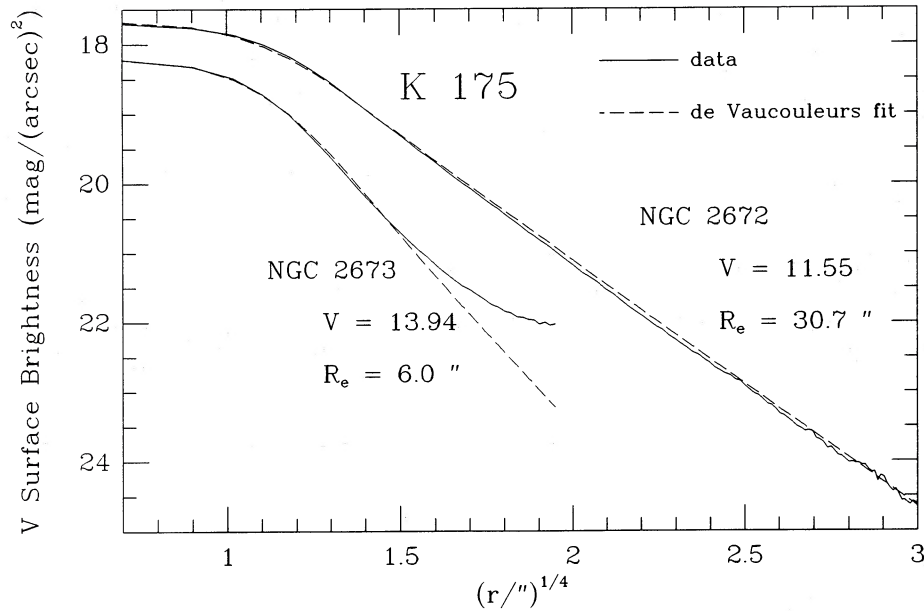


FIG. 4.—Azimuthally averaged surface brightness profiles for K175a and for K175b. A sector from each galaxy has been excluded in order to minimize contamination from the other galaxy. With each curve is a seeing-convolved best-fit $r^{1/4}$ profile, with best-fit parameters as given.

co-added into a single two-dimensional spectrum. Figure 5 (Plate 18) displays the fully processed K175 spectrum, covering the wavelength range 3875–4590 Å. Each pixel perpendicular to the dispersion corresponds to 1".7, slightly less than the slit width, which was 2". Note that the galaxy separation is 37", or 22 pixels. Pixels along the dispersion were defined in equal increments of $\log \lambda$, corresponding to equal steps in redshift with $\Delta v = 99.15 \text{ km s}^{-1}$; the FWHM of a typical line in the comparison spectrum was four pixels.

A late-type giant star observed with the same instrument setup was used as a template in the Fourier quotient program (hereafter FQP) in order to determine variations in rotation velocity and velocity dispersion as a function of position along the slit (see Sargent *et al.* 1977 for a discussion of the FQP; see Paper III for a description of its application to our investigation; and see Tonry 1985 for remarks about corrections to the KPNO FQP redshifts). Table 2 presents the FQP values for the redshifts and velocity dispersions measured at the centers of the two galaxies. The table also includes values for v_0 , the recession velocity corrected for the motion of the Sun relative to the centroid of the Local Group. These numbers can be

compared with redshifts reported by other authors. For K175a, we measure a correct recession velocity of $3729 \pm 16 \text{ km s}^{-1}$. Humason, Mayall, and Sandage (1956) measured $4109 \pm 100 \text{ km s}^{-1}$, while Tift (1982) found 4206 km s^{-1} . For K175b, we measure a corrected recession velocity of $3201 \pm 10 \text{ km s}^{-1}$. Humason, Mayall, and Sandage (1956) measured $3678 \pm 65 \text{ km s}^{-1}$ and Tift (1982) found 3850 km s^{-1} . Bieging and Biermann (1977) reported a corrected 21 cm H I redshift of 3850 km s^{-1} . Their value is 120 km s^{-1} higher than our redshift for K175a and 170 km s^{-1} higher than our luminosity-weighted average redshift of 3681 km s^{-1} ($\langle z \rangle = 0.01228$) for the pair. This gas was only marginally detected, and the source of this emission is not clear.

It is obvious that most of the recession velocity measurements quoted in the literature differ substantially from our values. This was not the case for other galaxies that we observed with the same instrument (see Paper III; Hoessel, Borne, and Schneider 1985). The reasons for the current discrepancy are not clear. However, we note that one can measure directly on Figure 5 a velocity difference of at least 450 km s^{-1} (our FQP value is 528 km s^{-1}), so we are confident that the

TABLE 2
REDSHIFTS, ABSOLUTE MAGNITUDES AND CENTRAL VELOCITY DISPERSIONS

SOURCE	NGC 2672				NGC 2673			
	cz	v_0^a	M_V	σ_0	cz	v_0	M_V	σ_0
This work	3843 ± 16	3729 ± 16	-22.40	258 ± 17	3315 ± 10	3201 ± 10	-20.00	134 ± 18
RC2	4223 ± 100	4109	3792 ± 65	3678
RSA	3983 ± 20	3869	-21.95
MK ^b	4200	...	-23.02	332 ± 24
T ^c	4206	3850
B ^d	3850

^a $\Delta v = 300 \sin i \cos b$.

^b Malumuth and Kirshner 1985.

^c Tift 1982.

^d Bieging and Biermann 1977.

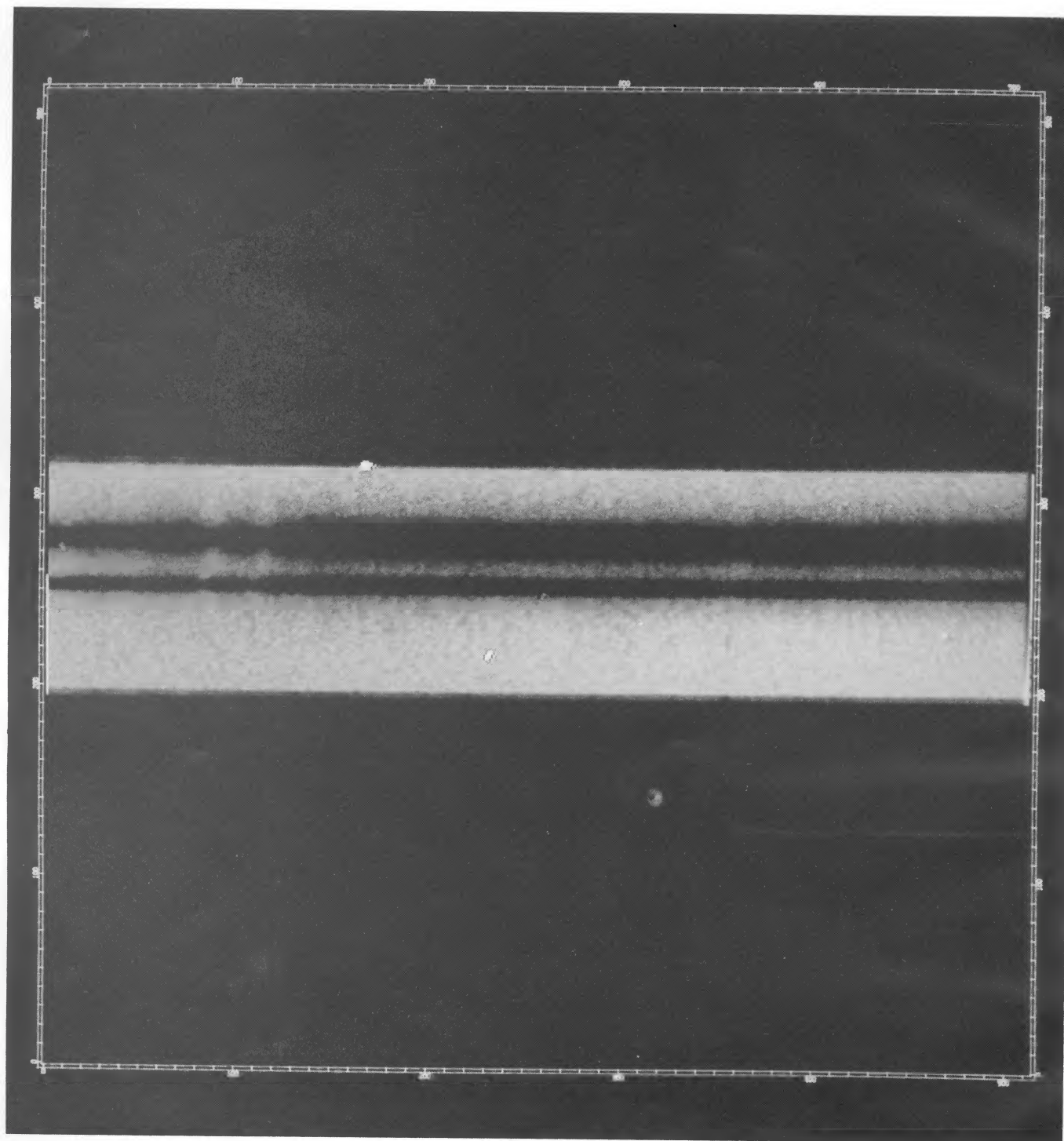


FIG. 5.—Print of the reduced two-dimensional long-slit spectrum of K175 with the slit across the two nuclei. Wavelength increases left to right, covering the range 3875–4590 Å with 512 pixels in equal increments of $\log \lambda$ ($=99.15 \text{ km s}^{-1}$). Perpendicular to the dispersion, the scale is $1''.7$ per pixel. K175a (west component) is at the top.

BALCELLS, BORNE, AND HOESSEL (*see* 336, 659)

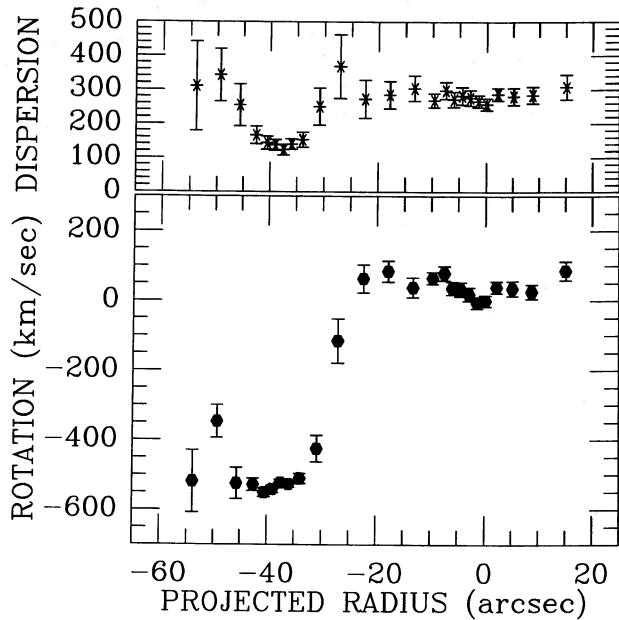


FIG. 6.—Line-of-sight rotation velocity and velocity dispersion profiles extracted from the spectrum shown in Fig. 5. The center of K175a is located at $R = 0$, while the center of K175b is located at $R = -37''$. Note the U-shaped rotation and dispersion profiles for K175b. Error bars of 1σ are shown.

relative velocity of the pair is significantly higher than that quoted by Tift (1982), and, therefore, that the pair is undergoing a high-velocity encounter.

Figure 6 presents the radial variations of mean line-of-sight velocity and velocity dispersion for K175 as extracted by the FQP from the reduced HGVS data. The velocity units are km s^{-1} , with rotation velocities measured with respect to the center of K175a. Projected radius is measured in arcseconds likewise from the center of K175a, increasing to the west. The center of K175b is located at $R_{\text{proj}} = -37''$. Along the line of sight, the true relative velocity of the pair is:

$$\Delta v_{\text{true}} = \Delta v_{\text{obs}} / (1 + \langle z \rangle) = 522 \pm 19 \text{ km s}^{-1}.$$

K175a shows very weak rotation ($V_{\text{max}}/\sigma_0 = 0.16$) in a retrograde direction with respect to the fast orbital motion. Such a slow rate is not unusual for an E2 galaxy (Illingworth 1981). K175a also shows a flat dispersion profile. Illingworth (1981) points out this may be an indication that M/L is increasing with radius inside such a galaxy, although Illingworth (1983) notes that an azimuthally elongated velocity ellipsoid, perhaps generated in the formation of the elliptical galaxy through the merger of two disk galaxies, can render the observed effect.

K175b shows no rotation near its center, but there is a suggestion in Figure 6 that its outer regions are moving away from the observer relative to the motion of its center. Apparent recession on both sides of the galaxy was discussed at length in Paper III for the galaxy pair K99. U-shaped velocity profiles are not unusual for interacting galaxies and very likely are a clear signature of tidal friction in action (Paper II). That conclusion appears at first to be somewhat weak in the case of K175 since the strong radial increases of both rotation and dispersion velocities in K175b may result from a superposition effect. However, at a projected radius $R = -27''$, the light contributed by K175a is very small (note the large errors on the velocities plotted at that radius in Fig. 6). At greater distances from the center of K175a, the contamination will be even

smaller, strongly diminishing the kinematic contribution of stars in K175a to the observed velocities for K175b. In fact, Figure 5 shows a clear gap between the spectral luminosity profiles of the two galaxies. Since tidal coupling and stripping are real consequences of gravitational interactions, and since U-shaped rotation and dispersion profiles are a natural result of these tides (see Paper III), the disturbances seen in the rotation and dispersion velocity profiles for K175b are probably intrinsic. They then owe their observed shapes mostly to the tidal coupling of the stars in K175b to the orbital motion of the galaxy pair. As described in Paper III, these U-shaped profiles are transient phenomena and will become unobservable one or two internal crossing times from now, as the galaxies separate.

IV. DYNAMICAL MODELS

The morphological characteristics, photometric parameters, rotation curves, and velocity dispersion profiles that were described in the previous sections represent the constraints on any model of the dynamical state of the K175 pair. In this section we present an interaction model for the binary that matches all of those observations. The search for the best-fit simulation proceeded along the same lines as in Papers IV and V (see Paper II for a full description of the method). Two observational characteristics made the modeling of K175 an interesting exercise: first, the high relative velocity of the pair, coupled to the very unusual rotation and velocity dispersion profiles in the secondary galaxy (NGC 2673), and, second, the two plumes emanating from the secondary. These features were used to constrain both the binary orbital parameters and the internal properties of the constituent galaxies, particularly those of the smaller galaxy. For all of the simulations described below, including our best-fit model, the mass ratio of the pair was assumed to be 10, approximately corresponding to the ratio of luminosities discussed in § IIc.

a) Constraints on the Binary Orbital Dynamics

The high relative velocity of the K175 pair implies a very rapid encounter. We found that the binary trajectory must be hyperbolic (i.e., unbound) both before and after the collision, and that the observer must be roughly aligned with the binary separation vector at the current epoch. This was required because the model has to match the observed ratio of relative velocity to internal dispersions, and at the same time the secondary has to appear projected superposed on the primary, at ~ 1.2 primary effective radii from the primary center (see Paper II for a detailed discussion on how velocities and the degree of superposition of the two galaxies determine the observer's viewing angle).

In Figure 7 we present the model rotation and dispersion profiles, plotted against the observations; the model values are plotted as double solid lines (plus/minus one standard deviation from the mean), and the observed values are indicated by the crosses (with error bars). The U-shaped dispersion profile across the secondary galaxy is nicely reproduced, as is the nearly flat, slightly U-shaped rotation curve, which is particularly gratifying given that our model for the secondary was that of a rapidly rotating elliptical. The lack of observed rotation was due to the coincidence that the slit was placed very nearly parallel to the galaxy's kinematic minor axis. That the observed velocity field, which is quite complex, was matched only for a limited range of binary encounters helped to constrain the final orbit solution. The plumes of K175b ultimately provided a strong constraint on the orbit also. It was clear that

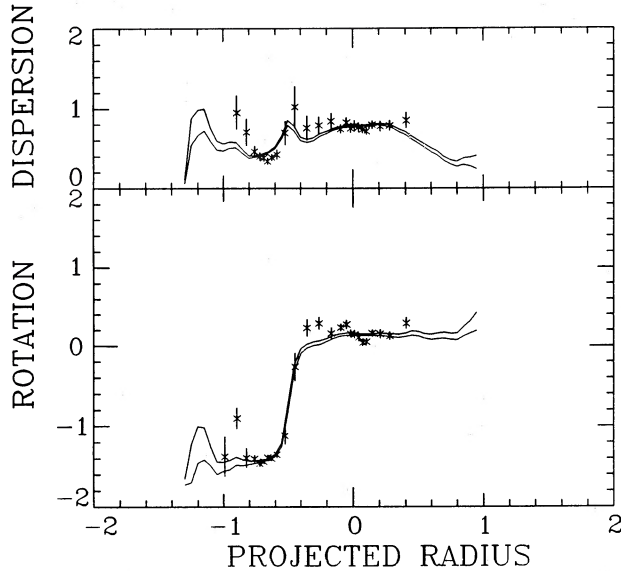


FIG. 7.—Superposition of the model rotation velocities and velocity dispersions onto the long-slit velocity data, drawn to scale. This is for our best simulation, as measured from the adopted viewing angle. Double solid lines are the model values (\pm one standard deviation). Observed velocities for K175 are identified by the crosses, with attached 1σ error bars.

the internal dynamics of K175b would be constrained by the presence of these features, but what was surprising was that the orbit (in particular, the impact parameter of the trajectory) was also tightly constrained by shapes of these tidal emanations. The fine tuning of the orbit is described in the next section following a discussion of the internal properties of K175b.

b) Constraints on the Internal Galaxy Dynamics

As mentioned above, the plumes on K175b (described in § IIb) are the most interesting morphological features of this interacting pair. The north plume is especially unusual for an E-E interaction. Unlike the broad fans of starlight seen in other E-E pairs (see Papers III and V), it is quite thin, and, taken together, the north and east plumes do not portray the typical S-pattern response of a rotating system to a tidal field (e.g., see TT72). Instead, the two plumes define a single arc, opening from K175b toward the NE. We discuss below how such a pattern constrains both the internal dynamics of K175b and the parameters of the binary orbit. A detailed discussion of how the plumes are generated is presented in § VI.

As discussed in TT72 and in Paper IV, a thin, coherent response to a tidal gravitational perturbation indicates a high degree of order in the internal motions of a galaxy. In contrast, a galaxy with little or no rotation responds incoherently to the perturbation, leading to a single broad stubby fan of tidally distended material (see examples in Papers IV and V). Consequently, the thin plumes emanating from K175b suggest that this must be a strongly rotating elliptical galaxy. What is the orientation of its rotation? In the previous section we determined that the observing viewing angle is close to the orbital plane. It is apparent therefore that the plumes are emerging out of the orbital plane. Since the tidal response of the stars in a strongly rotating galaxy grows primarily in the plane of their rotation (TT72), the plane of the rotation in K175b must therefore be at a significantly oblique angle to the orbital plane of the K175 pair. The actual orientation was determined from a series of experiments in which the secondary rotation axis was

varied. We now describe five of these simulations, which illustrate the main response patterns as a function of the orientation of the secondary spin and clarify how the spin orientation of K175b was found.

A mass ratio of 10 was used in all of these simulations, equal to the mass ratio used for the simulations of the real system. Our model for the secondary was that of a highly flattened oblate galaxy, fully rotationally supported (the *circular rotation mode* of MTBA; see Paper II). This mode was selected in order to emphasize the dependence of the tidal response on the spin direction. In all simulations, the primary was represented by a spherical nonrotating galaxy model (described in Paper I). The binary trajectory in each case was hyperbolic and was constrained to lie in the x - y plane, beginning on the positive x -axis. For the first four experiments, pericenter separation and speed were $R_{\text{per}} = 0.42$ and $V_{\text{per}} = 2.56$, respectively, while for the fifth simulation, $R_{\text{per}} = 0.15$ and $V_{\text{per}} = 3.2$. We follow the notation of TT72 to describe the secondary spin orientation: i denotes the inclination of the plane of internal rotation to the binary orbital plane, and ω denotes the argument of pericenter, measured in the plane of the orbit from the descending node of the rotation plane, increasing with binary orbital phase (see Fig. 6a of TT72). Inclinations 0° , 90° , and 180° were used in the spin experiments. When $i = 0^\circ$ or $i = 180^\circ$, the plane of internal rotation coincides with the plane of the binary orbit, and the value of ω is undefined. For the $i = 90^\circ$ case, the spin vector lies in the orbital plane, and four basic orientations of the spin vector are possible: the vector can point (a) toward the primary at pericenter ($\omega = -90^\circ$), (b) away from the primary at pericenter ($\omega = 90^\circ$), (c) in the direction of the orbital motion at pericenter ($\omega = 0^\circ$), or (d) in the direction opposite the orbital motion at pericenter ($\omega = 180^\circ$). Cases (a) and (b) are mirror symmetric, as are cases (c) and (d). We thus ran simulations for cases (b) and (d), as well as for $i = 0^\circ$ and $i = 180^\circ$. For the fifth experiment we used the same orientations as in (d) (with differing orbital parameters).

Figure 8 presents the results of the five spin experiments. Each row of boxes corresponds to one experiment and is labeled with the corresponding values of orbit inclination i and ω . In a given row, the first three boxes display three orthogonal views of the secondary particle distribution, from the three coordinate directions $-x$, $-y$, and $+z$. Where it appears, a circle is drawn, with radius = 0.10 (equal to twice the softening length, which is half the effective radius), representing the core of the primary galaxy. The primary was comprised of 9000 test particles, not drawn here, while the secondary was represented by 900 particles. The view from the $+z$ -direction includes a plot of the trajectory of the secondary galaxy in the orbital plane. The fourth box in each row presents a view of the pair from a position 20° above the orbital plane; this view includes the trajectory of the two galaxy centers in the orbital plane. For all five experiments, the snapshots in Figure 8 were taken when the binary separation was about ~ 0.9 length units, ~ 0.5 time units after pericenter.

Figure 8 will be discussed in more detail in § VI. Here we just note that tails extending out of the orbital plane are only obtained in the fourth and fifth spin experiments; such experiments are thus relevant to K175b. Two types of vertical extensions are obtained: an S-pattern (experiment 4) and a question mark “?” pattern (experiment 5). Of these two patterns, the S-pattern is the most common and appears for a wide range of pericenter separations and speeds. Only encounters with very small pericenter separations (not larger than

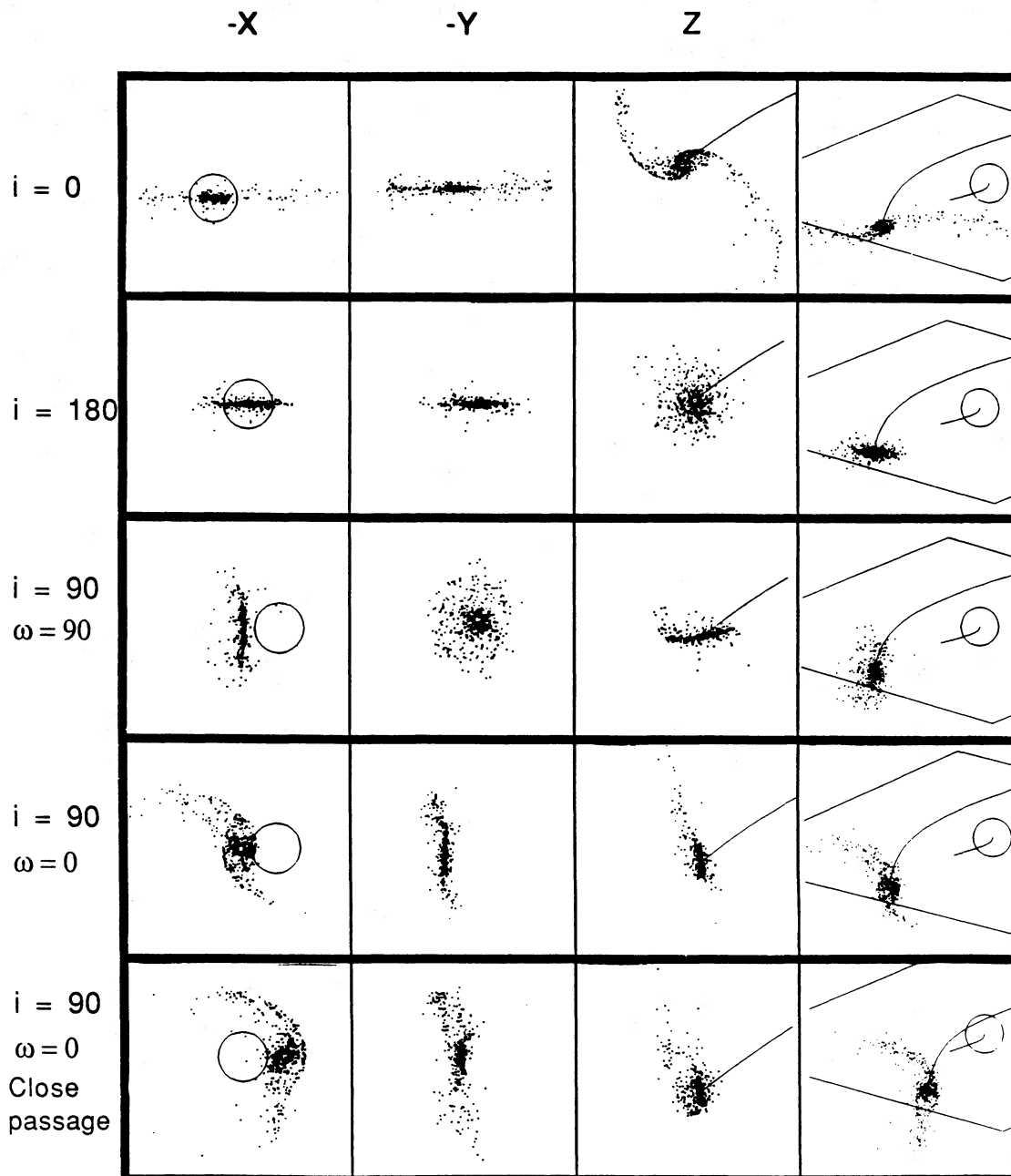


FIG. 8.—Morphological responses of a cold, rotating system to a perturber 10 times more massive, for five different orbital configurations. The first four of the five rows correspond to experiments with different orientations between target galaxy and orbital angular momenta, keeping all of the other orbital parameters fixed. The fifth experiment uses the same spin orientation as the fourth, but follows a different orbit, with a smaller pericenter separation and a faster pericenter speed. Each system is displayed at the same binary separation (≈ 0.9 length units). Three of the views are along the three orthogonal coordinate axes (boxes labeled “ $-x$,” “ $-y$,” and “ z ”), and the fourth view is that seen obliquely from an angle 20° above the orbital plane. The binary orbit lies in the x - y plane. Only those particles in the smaller, target galaxy are plotted. The location of the primary center of mass is represented by a circle whose radius (0.10 units) equals twice the model softening distance; the radius of the model primary galaxy is 1 length unit.

≈ 0.25) result in the “?”-pattern. When seen from $\sim 20^\circ$ below the orbital plane, the two tails in experiment 5 appear very similar to the plumes of K175b, with a strong, curved plume bending away from the primary, and a weaker, straight plume extending in a direction roughly orthogonal to the projected separation vector. A thorough, exhaustive investigation of a variety of simulations, using different spin orientations and binary orbital parameters, has convinced us that only simulations that are very similar to spin experiment 5 could produce

tails with the shape and orientation similar to the plumes observed in K175b. In particular, attempts to obtain a straight plume by looking at a curved feature from its plane of curvature proved unsuccessful. Therefore, we conclude that the encounter of the K175 pair had a very small pericenter distance, and that the spin of the secondary galaxy must have an orientation similar to our case (d), spin antiparallel to the secondary motion at pericenter.

The above experiments were run with the maximally rotat-

ing galaxy model. Essentially the same results are obtainable when a more realistic elliptical galaxy model is used to represent the secondary. We demonstrate this by repeating the fifth spin experiment (the "close passage" case) using an E4 secondary with $V_{\text{rot}}/\sigma_0 \approx 0.5$. Figure 9 displays the results of this experiment. The contour diagram presents the projected surface density distribution of all 9900 particles representing the two galaxies, observed 0.53 time units after pericenter passage, corresponding to the time when the simulation best matched all of our observations of K175. The particle distribution next to the contour map displays the secondary particles only, on the same scale as the contours, demonstrating that the extensions ("plumes") seen in the surface density mass distribution are composed of particles originating in the secondary galaxy. The other three boxes in Figure 9 present three

orthogonal views of the projected particle distribution in the secondary galaxy at the same model time. Since these three corresponding viewing angles are the same as those in Figure 8 ($-x$, $-y$, and $+z$), a comparison between the bottom row of that figure with these three plots reveals the effects of changing the internal galaxy parameters. We see in the views from $-x$ that the envelope of particles extending to the right of the secondary has the same orientation in both cases, demonstrating that the same physics is at work. However, the E4 galaxy, being a hot stellar system, has a much noisier (i.e., less sharp) response, and some of its stars now occupy the region between the two plumes. Similarly, light coming from the region between the plumes is seen in the real system.

We conclude (1) that K175b is a strongly rotating elliptical galaxy, (2) that it has just emerged from a very fast passage

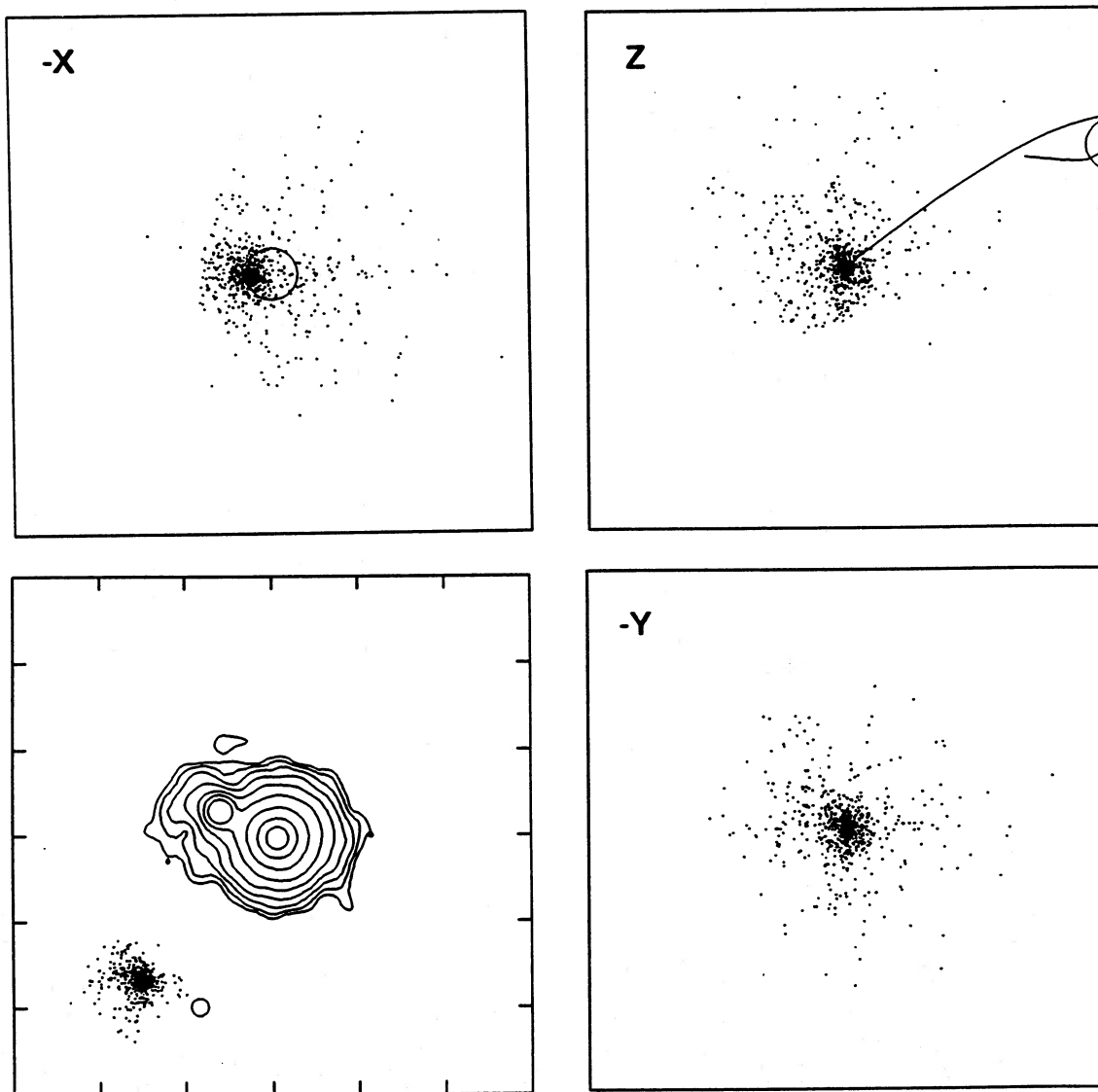


FIG. 9.—Lower left contour plot: our best simulation as seen from our adopted viewing angle. Compare with the contour diagram of the CCD imaging data (Fig. 2). The contours portray the surface density distribution of all test particles, whereas the small insert to the lower left shows only the particles in the target galaxy alongside the softening circle of the primary galaxy. Snapshots labeled " $-X$," " $-Y$," and " Z " correspond to views from those coordinate directions of our best simulation at the time when the model best matched the observational data. Only the secondary particles are shown here; the scale is 3 times that of the lower left snapshot. The binary orbit lies in the x - y coordinate plane, with the secondary galaxy initially placed on the $+x$ -axis, with a velocity directing it initially to smaller x and slightly larger y .

through the core of K175a, (3) that the binary orbital plane is approximately perpendicular to the plane of internal rotation in K175b, and (4) that the K175b spin vector was approximately antiparallel to the direction of motion of K175b at pericenter. Our model search procedure has allowed us to determine the orbital parameters of the encounter and the spin parameters of the secondary. The orbit parameters are $R_{\text{per}} = 0.15$ (pericenter separation), $V_{\text{per}} = 3.2$ (pericenter speed), and $T_{\text{per}} = 0.53$ (time since pericenter passage), assuming a mass ratio of 10:1. These numbers are translated into physical units in § VII, while their uncertainties are discussed in the following section.

V. UNCERTAINTIES IN THE ADOPTED SOLUTION

In the previous section we presented our adopted physical model of the K175 binary system. We will describe in this section just how well we have determined the various parameters that describe the K175 system. Within the context of our particular model, we will see that the parameters of the orbit and its spatial orientation are well constrained. As was the case in Papers IV and V for three other pairs of interacting ellipticals, a good determination of the dynamical mass of K175 follows from our adopted solution for the binary orbital and spatial configuration. On the other hand, because the observed velocities in K175a/b show little evidence for rotation in the line of sight, the precise rotation properties of the galaxies can only be deduced indirectly from their responses to the tidal perturbations, and consequently those properties are not as well constrained as those of the orbit.

Our simulations did not place strong constraints on the K175 binary mass ratio. The dynamical responses of the model galaxies to the tidal perturbations were similar in various experiments for which the mass ratio ranged from 4 to 20. Our adopted value ($= 10$) was derived from the observed luminosity ratio, assuming the same M/L in each galaxy. The problem is that the secondary is so much smaller that it renders almost no tidal damage to the primary, and hence the secondary offers very little indication of its actual mass. We argued in Paper V from the observed luminosity ratio of the NGC 4782/4783 pair and from the behavior of our simulations with the corresponding mass ratio that the two galaxies must have very similar M/L . We have no information with which to similarly constrain the components of K175.

For the pericenter velocity, a rather conservative upper limit to its uncertainty is $\pm 10\%$. At speeds below the acceptable range, the secondary slows down very quickly as a result of dynamical friction in the envelope of the primary, so that by the time the plumes become detectable, the line-of-sight relative velocity of the pair is too small to match that observed. At speeds above the allowed range, the secondary slows down too late in the encounter to allow a good match to the size and shape of the plumes. This upper limit on the speed is quite strong since all of these encounters are hyperbolic: faster orbits reach an asymptotic relative velocity higher than the observed value. Projection of the velocity vector to reduce its line-of-sight component does not help since one is forced to view the system very nearly parallel to the separation vector (which is nearly parallel to the velocity vector in hyperbolic trajectories) in order to match the small projected separation observed for the pair (1.2 effective radii).

For the pericenter separation R_{per} we have found a lower and an upper limit through our numerical experiments. The upper limit, at ~ 0.25 length units, is understandable in terms

of the difference between the fourth and fifth spin experiments shown in Figure 7: the plume pattern makes its transition from the “?” crescent shape to the S-shape near $R_{\text{per}} \sim 0.25$ (see § IVb). In fact, the straight north plume becomes a clearly defined feature only when the pericenter distance is significantly smaller than that limit. The lower limit on R_{per} is imposed by the observed relative strengths of the two plumes. It is apparent from Figure 3 that the curved east plume is brighter and more extended than the straight north plume. In our simulations, orbits that had a pericenter separation smaller than 0.1 resulted in the straight north plume being more prominent than the curved east plume. We therefore believe that the range $0.1 < R_{\text{per}} < 0.25$ strongly constrains the pericenter distance, with the best value (our adopted value) being $R_{\text{per}} = 0.15$. These limits are in fact model-dependent since they are set by the detailed behavior of the force field near the core of the primary galaxy. In particular, the value chosen for the primary softening radius affects the allowed range for R_{per} . Since the north plume actually becomes straight as a result of encountering a softened core potential (see § VI), the existence of the linear north plume on K175b offers a soft line of evidence to suggest a flattening in the K175a core density profile.

The internal properties of the galaxies are less well determined. We know that the primary K175a is slightly flattened (E2; see Fig. 2), and that it has a very small amount of internal rotation along the line of sight which is retrograde with respect to the relative trajectory of K175b (see Fig. 6). Its true three-dimensional flattening and degree of rotation are not known, and, because of the small mass of K175b, its response to the tidal perturbations are too weak to disclose any information on those properties. K175b, on the other hand, does respond well to the strong tidal perturbations imposed on it, and we can learn something about its internal workings. We are certain that it does rotate, with its spin vector lying very nearly in the orbital plane, pointing roughly in the direction opposite its motion at pericenter. Changing the inclination of the spin vector with respect to the orbital plane by 10° made the plume pattern in the secondary much more ill-defined. That pattern does not depend so strongly on ω (the azimuth of the spin vector in the orbital plane): changing that angle by 30° still resulted in a well-defined crescent-shaped plume pattern. The weak dependence on ω occurs because, in a close passage, the tidal action is effectively spread over a large range of orbital phases even in the impulse limit, since the orbital phase changes by $\approx 120^\circ$ during the period when the binary separation is smaller than one effective radius.

The actual strength of the secondary rotation is the least constrained of all our model input parameters. We are certain however that K175b does rotate, in spite of the absence of any detectable rotation in our velocity measurements. *Only a rapidly rotating stellar population can produce the plumes of Karachetsev 175b.* The existence of this rotation has been revealed solely in the response of K175b to the strong tidal perturbation imposed by K175a. Does the morphology of these tidal disturbances contain additional clues to the degree of rotation and/or flattening in K175b? Yes, but not very many. The plumes being fat and not very long and the presence of starlight in the region between the plumes suggest that these features have not developed from a cold disk, but from a hot rotating system. To address this issue directly, we ran several additional simulations, where the flattening of the secondary galaxy initial model ranged from E0 to E5, and the model rotation ranged from none to the maximum allowed rotation

speed (i.e., a fully rotationally supported model). Examination of this extensive series of models has convinced us that the nonrotating models cannot produce plumes. In order to obtain the plumes, we have to trade off rotation speed for flattening: the rounder the galaxy, the higher the minimum rotation speed at which the plumes in the secondary start to appear. In the end, we decided that K175b must be rotating fairly strongly, but that the degree of rotation cannot be stated with certainty.

The prominence of the plumes is certainly related to the degree of ordered internal motion in the secondary galaxy. But it is really a moot exercise attempting to infer the strength of rotation in the real galaxy from point-to-point comparisons with our simulations, since the S/N of the data far exceeds that of even our best models. While there are $\sim 10^{10}$ stars in the real secondary galaxy, and $\sim 300,000$ counts in the CCD image, there are only 900 test particles in our simulated galaxy with which we are trying to model some faint features in the CCD image, from which we are hoping to infer the internal dynamics of K175b. It is asking too much of our simulations to distinguish subtle differences in surface brightness from one plume to the other, or to ascertain what fraction of the tidally extended material actually lies in the region between the two plumes. We must recall that these are very weak features, with an integrated light some 20 times fainter than the total light from K175b.

Upon inspection, K175b appears to be an E0 galaxy. Do the rotation constraints imposed upon this galaxy suggest that it is peculiar in any sense? We think not. Our requirement that it be a rapid rotator does not contradict the observed lack of rotation along our slit since our viewing angle is not far from the direction of the spin vector and since the position angle of our slit is not far from the projected position angle of the axis of rotation. Therefore, neither an S0 morphology for K175b nor a cold rotating subsystem within that galaxy (e.g., an embedded disk) is required to explain the existence of the plumes, even though our models do not reject such possibilities. That K175b is a rapid rotator agrees with the conventional wisdom that small ellipticals spin rapidly (Davies *et al.* 1983). Only if K175b were truly spherical would we conclude that it is somewhat unusual, in the sense that our models would require $(V_{\max}/\sigma_0)_{\text{observed}} > (V_{\max}/\sigma_0)_{\text{oblate rotator}}$. In reality, several galaxies are known to have this property, one of which is the primary galaxy in the E-E pair K99 (see Papers III and IV). Our simulations actually indicated that the flattening of the model galaxies decreased during the interaction (i.e., the galaxies puffed up; see the $+z$ views in Figs. 8, 9, and 10). It is therefore possible that the amount of rotation required to generate the plumes was not excessive for the initial flattening of the secondary galaxy (i.e., the oblate rotator degree of rotation may not have been exceeded), and that the ellipticity of the galaxy has since decreased.

VI. PHYSICAL ORIGIN OF THE PLUMES

As we have seen, the plumes on K175b develop as a result of a gravitational encounter with a much more massive perturber whose orbit is inclined 90° to the plane of internal rotation. Therefore, unlike the traditional tidal tails of TT72, the tidal features seen in K175 were not created by a resonance between the motion of the perturber and the stellar orbits. In order to elucidate the mechanism that gave rise to the plumes, we examine here in some detail the different spin experiments displayed in Figure 8 (refer to § IVb for a general description of the figure). The orbital parameters used in the first four experi-

ments were identical, while a smaller pericenter separation and a larger pericenter speed were used for model (v). From top to bottom in Figure 8, the models correspond to (i) $i = 0^\circ$, parallel orbital and internal spins; (ii) $i = 180^\circ$, antiparallel orbital and internal spins; (iii) $i = 90^\circ$, $\omega = 90^\circ$, internal spin pointing toward the primary at pericenter; (iv) $i = 90^\circ$, $\omega = 0^\circ$, spin pointing opposite to the direction of secondary motion at pericenter; (v) same as (iv), except for the orbital parameters.

We discuss the experiments portrayed in Figure 8 in the context of the impulse approximation since the time that the secondary spends passing through the core of the primary is shorter than the stellar crossing time internal to the secondary. In this situation, the secondary does not appreciably change during this brief core passage when all of the tidal action occurs, and, consequently, the effects of the interaction can be argued in terms of the geometry of the system at pericenter.

Model (i): prograde orbit $i = 0^\circ$ (Fig. 8, first row).—In this experiment, the spin vector points out of the page in the $+z$ view. Long, thin tails develop in this case, caused by the strong resonance between the motion of a larger number of rotating particles and the orbit of the perturber. The tails grow in the plane of the orbit, developing into a characteristic S-shaped pattern. This well-known response occurs for any reasonable pericenter speed and separation.

Model (ii): retrograde orbit, $i = 180^\circ$ (Fig. 8, second row).—In this experiment, the spin vector points into the page in the view from $+z$. Here resonant coupling is nonexistent, and no tidal tails or bridges develop. This result is well-known from the work of TT72.

Model (iii): $i = 90^\circ$, $\omega = 90^\circ$ (Fig. 8, third row).—No coherent tidal response develops in this case either, which is what we expected since there is no resonance between the secondary rotation and the orbit of the primary perturber. At pericenter, there is no preferred position for the rotating particles in the secondary with respect to the perturber, and the passage is so fast that the expected coupling between the perturber and those secondary particles that are moving in the same direction as the perturber is irrelevant. As a result, the coherent motions in this rotating model galaxy do not result in a coherent response to the tidal perturbation.

Model (iv): $i = 90^\circ$, $\omega = 0^\circ$ (Fig. 8, fourth row).—In spite of the fact that the orbit is orthogonal to the plane of the rotation, a coherent S-pattern response appears in this experiment. It is due to the differential gravitational (i.e., tidal) field, which is quite strong owing to the high relative mass of the primary perturber. At pericenter, where most of the action occurs, the tidal field provides a centrifugal impulse of sufficient intensity to drive the outermost particles away from the main body of the secondary galaxy, which results in the observed spiral pattern. The relative intensity of the two tails depends on the pericenter distance. Note that the tail formation mechanism is physically quite different between cases (i) and (iv). The latter relies entirely on the centrifugal nature of the tidal field to force out the tails, whereas the former depends both on the tidal field and the resonant spin-orbit coupling to form the tails. Because of the absence of the spin-orbit resonance, and because of the short duration of the interaction when $i = 90^\circ$, we expect the centrifugal tidal mechanism of tail formation to be effective only in those $i = 90^\circ$ collisions involving very massive perturbers, as in the K175 pair.

Model (v): $i = 90^\circ$, $\omega = 0^\circ$, "close encounter" (Fig. 8, fifth row).—In this experiment, the spin vector points into the page when viewed from the $-x$ -direction. This is the only spin

orientation for which the response of the rotating secondary to the close passage of a massive perturber is qualitatively different for different pericenter separations. Two tails develop in all cases, except that the closest passages do not result in tails having the usual S-shape. Note the differing shapes of the lower tails in experiments (iv) and (v). We believe that this difference is due to the sign change of the perturber tidal field close to the center of the perturber, where the mass density is roughly constant. In the close passage case, the rotating secondary particles moving toward the perturber center of mass are initially accelerated toward that center, but at closest approach they receive a tidal impulse directed away from that center. These accelerated circulating particles then pass between the two galaxy centers, and continue to move downward away from the orbital plane. The perturber's tidal impulse has allowed them to escape the secondary gravitational field, just as in case (iv), but the absence of the normal tidal field causes them to evolve into a linear, instead of arch-shaped, pattern. Particles on the far side of the secondary with respect to the primary center of mass receive the normal outward tidal impulse and move away defining the usual curved pattern.

Figure 10 displays the time evolution of model (v) as viewed from the $-x$ and $+z$ directions. Each snapshot is labeled by the time t since pericenter, and includes a circle showing the position of the primary core: the radius of the circle is one-half of the effective radius (two softening radii). When viewed from the $-x$ -direction, the spin vector of the secondary points into the page. The first snapshot ($t = -0.095$) shows us that the secondary has suffered very little tidal damage at times very close to, but preceding, pericenter passage. A study of the model velocity field has similarly revealed a lack of tidal disturbances at this point. All of the effects of the tidal action will appear after pericenter. Immediately after pericenter ($t = 0.030$), the secondary still looks undisturbed, even though the tidal impulse has already modified the velocity structure: particles located in the lower left quadrant of the $-x$ projections have been accelerated to the left (by the tidal impulse), and they will form the curved upper plume. Particles located to the far right of the secondary in the $-x$ projections are within 0.05 length units from the primary center where the tidal field changes sign: these particles will receive a tidal impulse directed to the left (toward the center of the secondary, not away from it). Combined with their circulating motion around the secondary and their initial pull toward the center of the perturber, that impulse will allow these particles to form the straight lower plume. The development of this tail is most significant in the time between the second snapshot (taken immediately after pericenter) and the third, with the tail continuing to grow at subsequent times. We can understand from this discussion why the shape and strength of the lower tail is strongly dependent on the pericenter separation. No particles enter the reverse tide zone if the pericenter distance is too large, whereas smaller pericenter distances bring more particles into the core and produce a stronger tail.

By comparing the velocity structure of model (iv) with that of model (v) we can further understand the dynamical differences between these two cases. We display the model rotation curves in Figure 11. The top three panels display the rotation velocity profile for the secondary galaxy along the plane of rotation as seen from the $-y$ -direction in Figure 8. Negative abscissae correspond to the lower part of the galaxy ($z < 0$). The top panel presents the initial model velocity profile, which

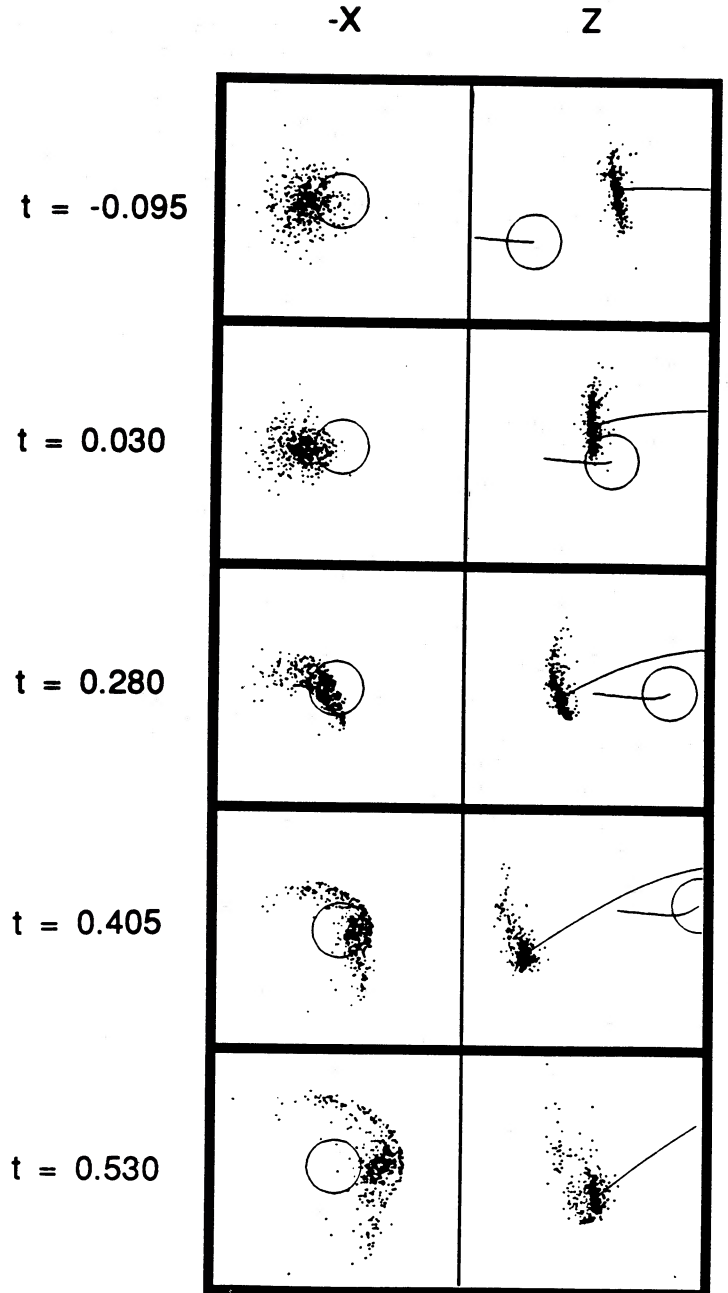


FIG. 10.—Views of the target galaxy in the fifth experiment of Fig. 8 as it interacts with the primary. Each row is labeled with the time since pericenter passage (1 model time unit = 53 million years). The spin vector of the rotating secondary is directed into the page for the “ $-x$ ” views.

was the same for both models (iv) and (v). The second panel displays the velocity profile from model (iv) after the interaction. While the rotation in the core remains unchanged, the systematic pattern is lost at the edges of the galaxy, where the rotation curve turns down, decreasing with increasing radius. Rotational disturbances seen on the left side of that velocity profile correspond to the lower tidal tail seen in the $-x$ view of Figure 8, and vice versa. The spiral S-pattern induced by the sheared velocity field will rotate as the tails expand until the tails finally dissipate. The third panel shows the velocity profile of the secondary from model (v), the close encounter experi-

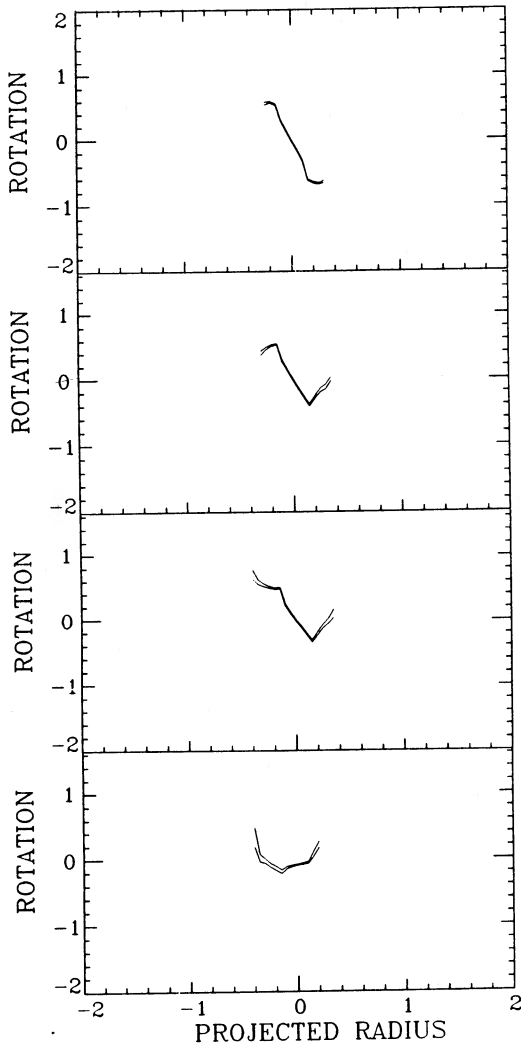


FIG. 11.—*Top panel:* edge-on rotation velocity profile of the secondary galaxy in experiments (iv) and (v) of Fig. 8 before the interaction. *Second panel:* velocity profile of the secondary galaxy in experiment (iv) after the interaction. *Third panel:* velocity profile of the secondary galaxy in the small-pericenter separation experiment (v) after the interaction. *Fourth panel:* velocity profile of the secondary galaxy alone in experiment (v) along the line connecting the galaxy centers from a view 20° below the orbital plane, and 45° out of the plane of secondary rotation. This view corresponds to that of our adopted solution for K175.

ment, after the interaction. The rotation velocity of the lower tail (at negative projected radius in Fig. 11) now increases outward with radius; as this tail moves out, it forms the linear plume.

We now relate the morphological differences between models (iv) and (v) with their kinematic differences, as shown in Figure 11. In model (iv) the rotating particles that have passed down between the two galaxies are pulled toward the primary. Hence, seen from the $-y$ -axis, the lower tail of that model (plotted at negative projected separations in Fig. 11) shows a turnover in its rotation velocity profile. Particles going up around the back of the secondary are pushed away from the center of the secondary by the usual tidal field, forcing those particles to move higher in that galaxy's potential well, thus diminishing their speeds as they extend outward into the tail. Hence the upper tail of model (iv) (plotted at positive projected

separations in Fig. 11) also shows a turnover in its rotation velocity profile. The strong shear in the rotation of model (iv) therefore leads to the observed spiral pattern in its tidal response to the perturbation. In model (v) the particles going up around the back of the secondary experience the same type of tidal impulse as do similar particles in model (iv), and therefore behave the same as those, leading both to the similar appearance of the two rotation curves at positive projected separations and to the similar form for the upper tails in those two models. On the other hand, the particles in model (v) that are passing down between the two galaxies can pass through one of two regimes. While at intermediate projected separations they respond to the same type of tidal impulse as do those particles in model (iv), resulting in a similar break in the rotation curve at intermediate negative abscissae, particles that are farther from the center of the secondary enter the reversed-tide zone and are pushed away from the perturber. That extra acceleration turns the rotation curve back up at large negative projected radii. This part of the curve corresponds to the straight lower tail. Its additional positive component of velocity will cause the “?”-pattern seen from the $-x$ view to rotate clockwise as the tails expand, and the bottom of the tail will slightly bend to the left.

The bottom panel in Figure 11 presents the velocity profile of the secondary particles in model (v) along the line connecting the primary and secondary centers, in a view that closely matches the position of the spectroscopic slit in our observations of the K175 pair. This curve was measured from the viewing angle and at the observation time that corresponds to our adopted solution for K175. The primary center of mass is at projected radius $+0.6$, while the secondary center is located at the origin. Velocities at negative projected radii include a contribution from the curved plume. Because no particles from the primary galaxy are included here, the U-shape cannot be the result of a superposition effect but must be an intrinsic property of the velocity field in the secondary galaxy immediately following the interaction. This provides an example of how U-shaped rotation curves can arise as a result of a tidal interaction. Such features were identified in Papers III and IV as a signature of tidal friction in action.

VII. SUMMARY

1. CCD surface photometry of the interacting pair of galaxies K175 has confirmed earlier measurements of the magnitude of K175a and has provided a reliable measure of the magnitude for K175b. Values are listed in Table 1, with the luminosity ratio of the two galaxies being 9:1. K175a is well fitted by a de Vaucouleurs law in the range from $2''$ – $80''$, covering $7 \text{ mag arcsec}^{-2}$ in surface brightness.

2. We confirm earlier photometric measurements which found that $B-V$ in each member of the pair to be normal for an elliptical galaxy. No measurable gradient in $B-V$ is found in either galaxy.

3. Photometric distortions in both galaxies indicate that the pair is interacting. The most prominent distortions are the two low surface brightness extensions (“plumes”) on K175b. Subtraction of the primary galaxy reveals the details of these features, whose shape and orientation are definitely peculiar for an elliptical galaxy. Distortions in K175a are in the form of small deviations from purely elliptical isophotes.

4. Line-of-sight velocities and velocity dispersions are derived from the application of the Fourier quotient technique to long-slit digital spectra. It is unclear from galaxy counts

whether a group exists around K175. In any case the measured relative velocity (522 km s^{-1}) is not unusually large for such a close pair of galaxies.

5. U-shaped rotation and velocity dispersion profiles are found in the secondary galaxy K175b. Such features were also present in the velocity structure of pairs previously studied by us (see Paper III). Our models support the conclusion that the profiles are of tidal origin, and are not the result of a superposition effect.

6. Numerical simulations of the binary were run using the multiple three-body algorithm (MTBA). Our models indicate that rapid rotation, with spin antiparallel to the direction of motion at pericenter, is required to produce the plumes on K175b. This conclusion is not inconsistent with the lack of measured rotation along the slit in the secondary. K175b is almost definitely a rapidly rotating elliptical galaxy, as are other low-luminosity ellipticals (Davies *et al.* 1983). Our spectroscopic slit was placed along the kinematic minor axis, hence the lack of measurable rotation. It is possible that the intrinsic flattening of K175b has been modified by the tidal interaction.

7. The north plume on K175b is straight, unlike typical tidal tails which are curved, most likely because the stars in the plume have passed through the core of the primary galaxy K175a where the direction of the tidal impulse changes sign. Those stars were therefore not drawn out of K175a on the usual sheared arc. Stars in the east plume of K175b have responded to the normal tidal impulse and hence form a curved tail.

8. The secondary came from the west and is now emerging from behind the primary core, with the time since pericenter passage being $\approx 2.3\text{--}2.8 \times 10^7$ yr. The pericenter separation must have been very small ($\approx 2.5 \text{ kpc} = 0.3$ primary effective radii) for the linear plume (to the north) to have the right shape and orientation. The trajectory before and after the close encounter is hyperbolic, so that, in the absence of dark matter, the pair is unbound. In the event that a group exists around K175, it is elongated, with K175 near one end and with four or

TABLE 3
RESULTS

Parameter	NGC 2672	NGC 2673	Systemic
Distance (Mpc)	61.35
Luminosity ($10^{10} L_{\odot}$)	5.65	0.619	6.27
Scale on the sky (kpc arcsec^{-1})	0.297
R_{eff} (kpc)	9.13	1.78	...
$\log(M/M_{\odot})$	11.62	10.62	11.67
$M/L_B (M_{\odot}/L_{\odot}^B)$	7
Projected separation (kpc)	11.0
Real separation (kpc)	15.0
Pericenter separation (kpc)	2.5
Time since pericenter (10^7 yr)	2.3–2.8

five other galaxies distributed linearly in the east-west direction. This could account for the large east-west velocity of K175b, allowing the pair to be bound within the group.

Our best-fit simulation constrains both the binary orbital parameters and the orientation of the pair on the sky, thus allowing for an accurate estimate of the dynamical mass of the system in the region immediately surrounding the two galaxies. We find $\log(M_1 + M_2) = 11.67$, which implies $M/L_B = 7$, assuming $M_1/M_2 = 10 \approx L_1/L_2$. Table 3 lists the main physical parameters of the K175 binary system. The model units used throughout the paper can be translated to physical units via these transformations: gravitational constant $G = 1$; one unit of length = 16.6 kpc; one unit of time = 5.3×10^7 yr; one unit of velocity = 306 km s^{-1} ; and one mass unit = $3.6 \times 10^{11} M_{\odot}$.

We are grateful to the Director of KPNO for the generous allocation of telescope time to this project. At the University of Wisconsin, partial support was provided through a subcontract to NASA contract NAS7-918. Partial support was also provided to one of us (M. B.) through the Space Telescope Science Institute visiting student program.

REFERENCES

- Biegging, J. H., and Biermann, P. 1977, *Astr. Ap.*, **60**, 361.
 Borne, K. D. 1984, *Ap. J.*, **287**, 503 (Paper I).
 ———. 1988a, *Ap. J.*, **330**, 38 (Paper II).
 ———. 1988b, *Ap. J.*, **330**, 61. (Paper IV).
 Borne, K. D., Balcells, M., and Hoessel, J. G. 1988, *Ap. J.*, **333**, 567 (Paper V).
 Borne, K. D., and Hoessel, J. G. 1988, *Ap. J.*, **330**, 51, (Paper III).
 Borne, K. D., and Richstone, D. O. 1988, preprint.
 Burstein, D. 1979, *Lick Obs. Bull.*, No. 826.
 Cutri, R. M., and McAlary, C. W. 1985, *Ap. J.*, **296**, 90.
 Davies, R. L., Efstathiou, G., Fall, S. M., Illingworth, G., and Schechter, P. L. 1983, *Ap. J.*, **266**, 41.
 Davis, L. E., and Seaquist, E. R. 1983, *Ap. J. Suppl.*, **53**, 269.
 Davoust, E., Paturel, G., and Vauglin, I. 1985, *Astr. Ap. Suppl.*, **61**, 273.
 de Vaucouleurs, G., de Vaucouleurs, A., and Corwin, R. 1976, *Second Reference Catalog of Bright Galaxies* (Austin: University of Texas Press).
 Dressel, L. L., and Condon, J. J. 1978, *Ap. J. Suppl.*, **36**, 53.
 Duncan, M. J., Farouki, R. T., and Shapiro, S. L. 1983, *Ap. J.*, **271**, 22.
 Farouki, R. T., and Shapiro, S. L. 1982, *Ap. J.*, **259**, 103.
 Ferretti, L., and Giovannini, G. 1980, *Astr. Ap.*, **92**, 296.
 Hoessel, J. G., Borne, K. D., and Schneider, D. P. 1985, *Ap. J.*, **293**, 94.
 Humason, M. L., Mayall, N. U., and Sandage, A. R. 1956, *A.J.*, **61**, 97.
 Illingworth, G. 1981, in *The Structure and Evolution of Normal Galaxies*, ed. S. M. Fall and D. Lynden-Bell (Cambridge: Cambridge University Press), p. 27.
 Illingworth, G. 1983, in *IAU Symposium 100, Internal Kinematics and Dynamics of Galaxies*, ed. E. Athanassoula (Dordrecht: Reidel), p. 257.
 Karachentsev, I. D. 1972, *Comm. Special Ap. Obs. USSR*, **7**, 3.
 Kormendy, J., and Illingworth, G. 1982, *Ap. J.*, **256**, 460.
 Landolt, A. V. 1973, *A.J.*, **78**, 959.
 Miller, R. H., and Smith, B. F. 1980, *Ap. J.*, **235**, 421.
 Malumuth, E. M., and Kirshner, R. P. 1985, *Ap. J.*, **291**, 8.
 Ostriker, J. P., Spitzer, L., Jr., and Chevalier, R. A. 1972, *Ap. J. (Letters)*, **176**, L51.
 Quinn, P. J., and Goodman, J. 1986, *Ap. J.*, **309**, 472.
 Sargent, W. L. W., Schechter, P. L., Boksenberg, A., and Shorridge, K. 1977, *Ap. J.*, **212**, 326.
 Tift, W. G. 1982, *Ap. J. Suppl.*, **50**, 319.
 Toomre, A., and Toomre, J. 1972, *Ap. J.*, **178**, 623.
 Villumsen, J. V. 1982, *M.N.R.A.S.*, **199**, 493.
 White, S. D. M. 1978, *M.N.R.A.S.*, **184**, 185.
 ———. 1979, *M.N.R.A.S.*, **189**, 831.
 ———. 1982, in *Morphology and Dynamics of Galaxies*, (ed. L. Martinet and M. Mayor (Geneva: Geneva Observatory), p. 289.

MARC BALCELLS and JOHN G. HOESSEL: Washburn Observatory, University of Wisconsin, 475 North Charter Street, Madison, WI 53706

KIRK D. BORNE: Space Telescope Science Institute, 3700 San Martin Drive, Homewood Campus, Baltimore, MD 21218